Source-receiver Marchenko redatuming on field data using an adaptive double-focusing method

Staring, Myrna; Pereira, Roberto; Douma, Huub; Van Der Neut, Joost; Wapenaar, Kees

DOI
10.1190/geo2017-0796.1

Publication date
2018

Document Version
Final published version

Published in
Geophysics

Citation (APA)
Staring, M., Pereira, R., Douma, H., Van Der Neut, J., & Wapenaar, K. (2018). Source-receiver Marchenko redatuming on field data using an adaptive double-focusing method. *Geophysics*, *83*(6), S579-S590. https://doi.org/10.1190/geo2017-0796.1

GEOPHYSICS, VOL. 83, NO. 6 (NOVEMBER-DECEMBER 2018); P. S579–S590, 13 FIGS.
10.1190/GEO2017-0796.1

Source-receiver Marchenko redatuming on field data using an adaptive double-focusing method

Myrna Staring[1], Roberto Pereira[2], Huub Douma[3], Joost van der Neut[4], and Kees Wapenaar[1]

ABSTRACT

We have developed an adaptive double-focusing method that is specifically designed for the field-data application of source-receiver Marchenko redatuming. Typically, the single-focusing Marchenko method is combined with a multidimensional deconvolution (MDD) to achieve redatuming. Our method replaces the MDD step by a second focusing step that naturally complements the single-focusing Marchenko method. Instead of performing the MDD method with the directionally decomposed Green's functions that result from single-focusing, we now use the retrieved upgoing Green's function and the retrieved downgoing focusing function to obtain a redatumed reflection response in the physical medium. Consequently, we only remove the strongest overburden effects instead of removing all of the overburden effects. However, the gain is a robust method that is less sensitive to imperfections in the data and a sparse acquisition geometry than the MDD method. In addition, it is computationally much cheaper, more straightforward to implement, and it can be parallelized over pairs of focal points, which makes it suitable for application to large data volumes. We evaluate the successful application of our method to 2D field data of the Santos Basin.

INTRODUCTION

The Santos Basin offshore Brazil is an excellent example of a region where internal multiples hinder accurate imaging (Cypriano et al., 2015). The region contains presalt carbonates that often hold significant amounts of oil. These carbonates are covered by a highly reflective stratified salt layer that generates strong internal multiples. Moreover, the concave shape of the salt focuses the energy and thereby further enhances these multiples.

Most conventional imaging methods, for example, reverse time migration (RTM), are based on the assumption that the recorded wavefield consists of single-scattered waves. This assumption is not met in reality, which leads to imaging artifacts in areas with a complex overburden that generates strong internal multiples. Figure 1 shows RTM images of the Santos Basin, where the artifacts due to multiples generated in the overburden are clearly visible. Imaging in the Santos Basin, or in similar geologic settings, could significantly benefit from the removal of internal multiples.

Various methods exist that aim to predict and remove internal multiples from the reflection response (Weglein et al., 1997; Jakubowicz, 1998; Hung and Wang, 2012). Other methods aim to address multiples during imaging, such as full-waveform imaging (Davydenko and Verschuur, 2017) and Marchenko imaging. Our focus is on the Marchenko method, which was first introduced in geophysics by Broggini and Snieder (2012), based on the work of Rose (2001, 2002). Wapenaar et al. (2013) modify the method and extend it to more dimensions.

The Marchenko method is data-driven, only requiring the reflection response at the acquisition surface and a smooth velocity model of the subsurface. It aims to solve the coupled Marchenko equations, which results in focusing functions. These focusing functions, in turn, relate the wavefield measured at the acquisition surface to directionally decomposed Green's functions at specified virtual receiver positions (coinciding with the focal points of the focusing functions) inside the medium. These Green's functions contain all orders of internal multiples and can be used to create a redatumed reflection response directly above the target area.

There are multiple ways of obtaining a source-receiver redatumed reflection response from the retrieved focusing functions and Green's

Manuscript received by the Editor 7 December 2017; revised manuscript received 19 July 2018; published ahead of production 03 September 2018; published online 29 November 2018.
[1]Delft University of Technology, Department of Geoscience and Engineering, Stevinweg 1, Delft 2628 CN, The Netherlands. E-mail: m.staring-2@tudelft.nl; c.p.a.wapenaar@tudelft.nl.
[2]CGG, Av. Pres. Wilson, 231 — Centro, Rio de Janeiro — RJ 20030-020, Brazil. E-mail: roberto.pereira@cgg.com.
[3]E-mail: huub.douma@gmail.com.
[4]Delft University of Technology, Department of Imaging Physics, Laboratory of Acoustical Wavefield Imaging, Lorentzweg 1, Delft 2628 CJ, The Netherlands. E-mail: j.r.vanderneut@tudelft.nl.

functions (van der Neut et al., 2018). Because the Green's functions are already "receiver redatumed" (see Figure 2b), the source also needs to be brought down to obtain a source-receiver redatumed reflection response (Figure 2c). Conventionally, a multidimensional deconvolution (MDD) of the retrieved upgoing Green's function with the retrieved downgoing Green's function is used to achieve this (Wapenaar et al., 2014b). In this case, the resulting source-receiver redatumed reflection response exists in a truncated medium. This response is free of internal multiples generated in the overburden and can be used to create an image of the target area that is free of artifacts due to these multiples. However, solving the MDD method requires solving a large-scale inverse problem that is fundamentally ill-posed (Minato et al., 2013). This makes the method sensitive to imperfections in the data (e.g., noise or incomplete illumination) and sparse acquisition geometries, which we typically find in field data. Because our aim is to apply source-receiver Marchenko redatuming to field data, we decided to look for an alternative source redatuming approach that is more suitable for our needs.

In this paper, we present the adaptive double-focusing method. Starting from the preprocessing of the acquired reflection response, we go through the theory of the Marchenko method step by step to redatum our receivers. After that, we review the MDD method and discuss its advantages and limitations. Based on this review, we introduce the adaptive double-focusing method and explain why this method is more suitable for applying source-receiver Marchenko redatuming to field data. Then, we bring the theory into practice by performing a series of tests on 2D synthetic data and 2D field data. We compare the performance of the adaptive double-focusing method with the performance of the MDD method on 2D synthetic data for three different cases: for a dense acquisition geometry and a known scaling factor, for a dense acquisition geometry and an unknown scaling factor, and for a coarse acquisition geometry and a known scaling factor. The results of these tests clearly show the benefits of the second focusing step of the adaptive double-focusing method over the conventionally used MDD method for source redatuming. We conclude this paper by demonstrating the successful application of the proposed method to 2D field data of the Santos Basin. The adaptive double-focusing method correctly predicts and subtracts internal multiples, which results in a much cleaner image and an improvement of the geologic interpretability in the target area.

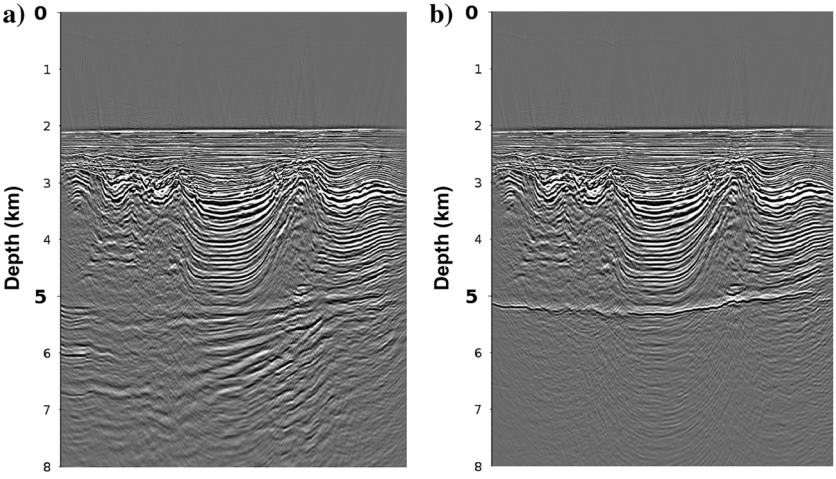

Figure 1. (a) The RTM image of the 2D synthetic data of the Santos Basin. (b) The same image, but the model is homogeneous below the base of salt such that only internal multiples generated in the overburden are visible below the base of salt.

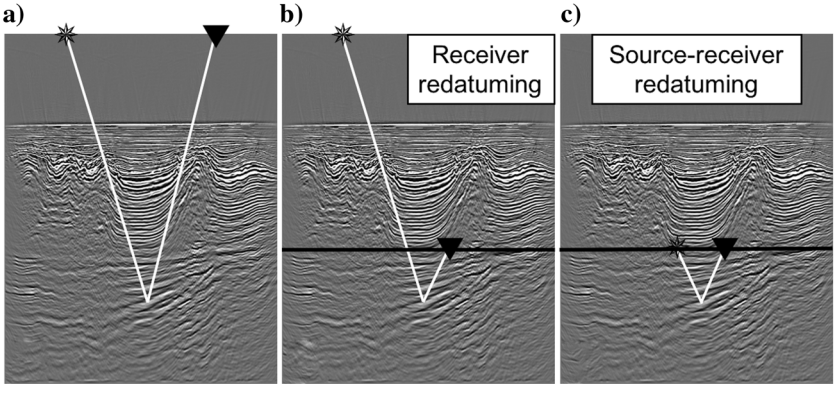

Figure 2. (a) Rays indicating the reflection response recorded by sources and receivers at the acquisition surface, (b) rays indicating receiver redatuming, and (c) rays indicating source-receiver redatuming. The seismic images in the background are only meant to illustrate an inhomogeneous medium; it is the same in all subfigures.

RECEIVER REDATUMING

We start with reflection response $R(\mathbf{x}_R, \mathbf{x}_S, t)$ that accounts for propagation and scattering from sources $\mathbf{x}_S$ at the acquisition surface $\partial\mathbb{D}_0$ via the inhomogeneous lower half-space to receivers $\mathbf{x}_R$ at the acquisition surface $\partial\mathbb{D}_0$. It is assumed that the half-space above $\partial\mathbb{D}_0$ is reflection free. This situation is achieved for streamer data by suppressing surface-related multiples, removing noise, horizontally propagating waves, and the receiver ghost, and by deconvolving the source signature. For ocean-bottom cable (OBC) data, we achieve this situation by applying a MDD (e.g., Amundsen et al., 2001). Using the preprocessed reflection response R, we introduce operator $\mathcal{R}$:

$$\mathcal{R}P(\mathbf{x}_R,t) = \int_{\partial\mathbb{D}_0} R(\mathbf{x}_R,\mathbf{x}_S,t) * P(\mathbf{x}_S,t)\,d^2\mathbf{x}_R. \tag{1}$$

Operator $\mathcal{R}$ performs a multidimensional convolution of the reflection data R with an arbitrary wavefield $P(\mathbf{x}_S, t)$. We also introduce operator $\mathcal{R}^\star$ that performs a multidimensional correlation of the reflection response R with arbitrary wavefield P:

$$\mathcal{R}^\star P(\mathbf{x}_R, t) = \int_{\partial\mathbb{D}_0} R(\mathbf{x}_R, \mathbf{x}_S, -t) * P(\mathbf{x}_S, t)\,d^2\mathbf{x}_R. \tag{2}$$

Next, we use these operators in the Marchenko method. At the core of this method are the directionally decomposed focusing functions $\widehat{f}^{+}(\mathbf{x}_S, \mathbf{x}_F, t)$ and $\widehat{f}^{-}(\mathbf{x}_S, \mathbf{x}_F, t)$. They relate the reflection response $R(\mathbf{x}_R, \mathbf{x}_S, t)$ measured at the acquisition surface $\partial\mathbb{D}_0$ to the directionally decom-

posed Green's functions $\widehat{G}^{+}(\mathbf{x}_F, \mathbf{x}_S, t)$ and $\widehat{G}^{-}(\mathbf{x}_F, \mathbf{x}_S, t)$ measured at the redatuming level $\partial\mathbb{D}_i$ (Wapenaar et al., 2013; Slob et al., 2014; van der Neut et al., 2015):

$$\widehat{f}^{-}(\mathbf{x}_S, \mathbf{x}_F, t) + \widehat{G}^{-}(\mathbf{x}_F, \mathbf{x}_S, t) = \mathcal{R}\widehat{f}_0^{+}(\mathbf{x}_S, \mathbf{x}_F, t) + \mathcal{R}\widehat{f}_m^{+}(\mathbf{x}_S, \mathbf{x}_F, t) \quad (3)$$

and

$$\widehat{f}_0^{+}(\mathbf{x}_S, \mathbf{x}_F, t) + \widehat{f}_m^{+}(\mathbf{x}_S, \mathbf{x}_F, t) - \widehat{G}_d^{+}(\mathbf{x}_F, \mathbf{x}_S, -t) - \widehat{G}_m^{+}(\mathbf{x}_F, \mathbf{x}_S, -t) = \mathcal{R}^{\star}\widehat{f}^{-}(\mathbf{x}_S, \mathbf{x}_F, t). \quad (4)$$

Here, the symbol $\widehat{\ }$ denotes a band limitation and the $+$ and $-$ represent the downgoing and upgoing wavefields recorded at virtual receivers. Vector $\mathbf{x}_F$ denotes the focal points that will become virtual receivers located at the redatuming level $\partial\mathbb{D}_i$. Evanescent waves are neglected in equation 4. The resulting Green's functions account for propagation through the inhomogeneous lower half-space from a source at the acquisition surface $\mathbf{x}_S$ to a focal point $\mathbf{x}_F$ at the redatuming level, and they are thus considered receiver-redatumed wavefields (see Figure 2b). These Green's functions correctly contain all orders of scattering generated in the overburden. Note that the downgoing Green's function $\widehat{G}^{+}$ has a direct part $\widehat{G}_d^{+}$ and a multiple coda $\widehat{G}_m^{+}$. In addition, the downgoing focusing function consists of a direct part $\widehat{f}_0^{+}$ and a coda $\widehat{f}_m^{+}$. The direct part $\widehat{f}_0^{+}$ is equal to the inverse of the direct arrival of the transmission response of the overburden, which can be estimated from a smooth velocity model (Broggini et al., 2014). It can be obtained by finite-difference modeling or by using an eikonal solver. The wavefield $\widehat{f}_0^{+}$ has been convolved with a zero-phase wavelet that covers the finite frequency content of the data, such that a band limitation is imposed. The coda $\widehat{f}_m^{+}$ follows the direct wave $\widehat{f}_0^{+}$ and accounts for the scattering effects of the overburden. If the overburden was homogeneous, this coda would not exist and the focusing function would only have a direct part.

The key element in solving equations 3 and 4 is a causality assumption, which presumes that the focusing function and the Green's function are separated in the time domain (Wapenaar et al., 2014b). A Green's function is causal by definition (the first arrival is at $t = t_d$, followed by the scattering coda), whereas a focusing function is acausal (arriving before $t = t_d$, nonphysical). We design a time window $\theta(\mathbf{x}_F, \mathbf{x}_S, t)$ such that it separates the causal and acausal wavefields in the time domain:

$$\theta(\mathbf{x}_F, \mathbf{x}_S, t) = \theta_0(t + t_d(\mathbf{x}_F, \mathbf{x}_S) - t_\varepsilon) - \theta_0(t - t_d(\mathbf{x}_F, \mathbf{x}_S)) + t_\varepsilon). \quad (5)$$

The truncations applied by this window are Heaviside step functions θ_0 based on the one-way traveltime t_d from the acquisition surface to the focal point. The term t_ε corrects for the finite frequency content of the data. As a rule of thumb, it is equal to half the duration of the zero-phase wavelet that was placed on the direct wave $\widehat{f}_0^{+}$ (Slob et al., 2014). We explain in Appendix A how to choose t_ε such that the time window $\theta(\mathbf{x}_F, \mathbf{x}_S, t)$ is correctly designed.

We obtain the coupled Marchenko equations by applying time window $\theta(\mathbf{x}_F, \mathbf{x}_S, t)$ to equations 3 and 4:

$$\widehat{f}^{-}(\mathbf{x}_S, \mathbf{x}_F, t) = \theta(\mathbf{x}_F, \mathbf{x}_S, t)\mathcal{R}\widehat{f}_0^{+}(\mathbf{x}_S, \mathbf{x}_F, t) + \theta(\mathbf{x}_F, \mathbf{x}_S, t)\mathcal{R}\widehat{f}_m^{+}(\mathbf{x}_S, \mathbf{x}_F, t) \quad (6)$$

and

$$\widehat{f}_m^{+}(\mathbf{x}_S, \mathbf{x}_F, t) = \theta(\mathbf{x}_F, \mathbf{x}_S, t)\mathcal{R}^{\star}\widehat{f}^{-}(\mathbf{x}_S, \mathbf{x}_F, t). \quad (7)$$

Convolutions and correlations along the time axis can be efficiently carried out by multiplications in the frequency domain. Conversely, the time-windowing operations are more efficiently carried out in the time domain. When comparing equations 3 and 4 to equations 6 and 7, the effect of the time window $\theta(\mathbf{x}_F, \mathbf{x}_S, t)$ becomes clear. The Green's functions $\widehat{G}^{-}$ and $\widehat{G}^{+}$ and the direct downgoing focusing function $\widehat{f}_0^{+}$ have been muted such that only the coda of the downgoing focusing function $\widehat{f}_m^{+}$ and the upgoing focusing function $\widehat{f}^{-}$ remains on the left side of the equations. The number of unknowns has been reduced to these two focusing functions only such that the coupled Marchenko equations can be iteratively solved, given that $\widehat{f}_0^{+}$ is known. The iterative process is initiated by solving equation 6, using the direct part of the time-reversed wave $\widehat{f}_0^{+}$ and setting $\widehat{f}_m^{+} = 0$.

Once initiated, the iterative process alternates between updating the upgoing focusing function $\widehat{f}^{-}$ and the coda of the downgoing focusing function $\widehat{f}_m^{+}$. When converged, the focusing function focuses at the defined focal point, which then acts as a virtual receiver. Alternatively, this set of equations can be solved by direct inversion (Ravasi, 2017; Slob and Wapenaar, 2017).

We apply the time window $\Psi(\mathbf{x}_F, \mathbf{x}_S, t) = 1 - \theta(\mathbf{x}_F, \mathbf{x}_S, t)$ to retrieve the upgoing Green's function $\widehat{G}^{-}$ from equation 3:

$$\widehat{G}^{-}(\mathbf{x}_F, \mathbf{x}_S, t) = \Psi(\mathbf{x}_F, \mathbf{x}_S, t)\mathcal{R}\widehat{f}_0^{+}(\mathbf{x}_S, \mathbf{x}_F, t) + \Psi(\mathbf{x}_F, \mathbf{x}_S, t)\mathcal{R}\widehat{f}_m^{+}(\mathbf{x}_S, \mathbf{x}_F, t). \quad (8)$$

However, the time window $\Psi(\mathbf{x}_F, \mathbf{x}_S, t)$ is not sufficient to retrieve the downgoing Green's function $\widehat{G}^{+}$ from equation 4. When applying this filter to equation 4, we would not only retrieve $\widehat{G}^{+}$, but also the direct part of the downgoing focusing function $\widehat{f}_0^{+}$. This is due to the fact that the time-reversed direct part of the downgoing Green's function $\widehat{G}_d^{+}$ and the direct part of the downgoing focusing function $\widehat{f}_0^{+}$ overlap in time. Therefore, we use the retrieved focusing functions $\widehat{f}^{-}$ and $\widehat{f}^{+}$ (Wapenaar et al., 2014b):

$$\widehat{G}^{+}(\mathbf{x}_F, \mathbf{x}_S, -t) = -\mathcal{R}^{\star}\widehat{f}^{-}(\mathbf{x}_S, \mathbf{x}_F, t) + \widehat{f}^{+}(\mathbf{x}_S, \mathbf{x}_F, t). \quad (9)$$

This concludes our review of how to retrieve focusing functions $\widehat{f}^{+}(\mathbf{x}_S, \mathbf{x}_F, t)$ and $\widehat{f}^{-}(\mathbf{x}_S, \mathbf{x}_F, t)$ and receiver-redatumed Green's functions $\widehat{G}^{+}(\mathbf{x}_F, \mathbf{x}_S, t)$ and $\widehat{G}^{-}(\mathbf{x}_F, \mathbf{x}_S, t)$ using the Marchenko method. In the following, we use these retrieved wavefields as input for source redatuming.

SOURCE REDATUMING: The MDD METHOD

Conventionally, the second redatuming step is achieved by a MDD. This method is inherited from seismic interferometry, in which it was used for virtual source redatuming, interferometric imaging, or to retrieve a reflection response from passive data (e.g., van der Neut et al., 2011; Nakata et al., 2014; Hartstra et al., 2017). In the preprocessing of the reflection response, it can also be used to

remove surface-related multiples, the source signature, and ghosts from OBC data (Amundsen et al., 2001). The following relation holds between the receiver-redatumed Green's functions and the redatumed reflection response R:

$$\widehat{G}^{-}(\mathbf{x}_F,\mathbf{x}_S,t)=\int_{\partial\mathbb{D}_i} R(\mathbf{x}_F,\mathbf{x}'_F,t)*\widehat{G}^{+}(\mathbf{x}'_F,\mathbf{x}_S,t)d^2\mathbf{x}'_F, \quad (10)$$

where x_F and x'_F indicate the focal points at the redatuming level $\partial\mathbb{D}_i$. By deconvolving the Green's functions, we obtain the redatumed reflection response $R(\mathbf{x}_F,\mathbf{x}'_F,t)$ that accounts for propagation from virtual sources to virtual receivers at depth level $\partial\mathbb{D}_i$. This response is measured in a truncated medium that is reflection free above the redatuming level (see Figure 3a). However, we need to solve a large-scale inverse problem to find the redatumed reflection response R that resides inside the integrand. This inverse problem is fundamentally ill-posed (Minato et al., 2013), and it has to be stabilized to be successfully solved. In field data, we typically have incomplete illumination, a sparse acquisition geometry, a finite aperture, and noise. These factors contribute to the instability of the MDD method such that it becomes more difficult to obtain a correct solution to the inverse problem (van der Neut et al., 2011). Therefore, we decided to look for an alternative method that does not require solving an inverse problem. We remark that the MDD method is successfully used in a range of other applications, and that we simply look for an alternative that is more suitable for our needs.

AN ALTERNATIVE: THE ADAPTIVE DOUBLE-FOCUSING METHOD

Solving the coupled Marchenko equations can be considered a first focusing step (bringing the receivers down), and we now propose to replace the inversion step of the MDD method by a second focusing step (bringing the sources down). Instead of using the directionally decomposed Green's functions $\widehat{G}^{-}$ and $\widehat{G}^{+}$ to perform the MDD method, we select the upgoing Green's function $\widehat{G}^{-}$ and the downgoing focusing function $\widehat{f}^{+}$ for a more simple and straightforward source-redatuming scheme. When convolving the downgoing focusing function $\widehat{f}^{+}(\mathbf{x}_S,\mathbf{x}'_F,t)$ at a virtual source location with the upgoing Green's function $\widehat{G}^{-}(\mathbf{x}_F,\mathbf{x}_S,t)$ at a virtual receiver location, we create downward-radiating virtual sources at the redatuming level (Wapenaar et al., 2016; Singh and Snieder, 2017; van der Neut et al., 2018):

$$\widehat{\widehat{G}}^{-+}(\mathbf{x}_F,\mathbf{x}'_F,t)=\int_{\partial\mathbb{D}_0}\widehat{G}^{-}(\mathbf{x}_F,\mathbf{x}_S,t)*\widehat{f}^{+}(\mathbf{x}_S,\mathbf{x}'_F,t)d^2\mathbf{x}_S, \quad (11)$$

where $\widehat{\widehat{G}}^{-+}(\mathbf{x}_F,\mathbf{x}'_F,t)$ is the upgoing wavefield measured by virtual receivers at $\mathbf{x}_F$ due to downgoing virtual sources at $\mathbf{x}'_F$. The virtual sources have to be located slightly above the virtual receivers for this relation to hold. Note that the redatumed response $\widehat{\widehat{G}}^{-+}$ has to be deconvolved with the autoconvolution of the user-specified zero-phase wavelet on the direct wave $\widehat{f}^{+}_0$. This is needed to remove the double band limitation that stems from the convolution of two wavefields that are both wavelet dressed in equation 11.

We can now achieve source redatuming without the need for an inversion (and its accompanying stabilization). This should make the double-focusing method less sensitive to imperfections that are typically found in field data. In addition, double focusing is computationally cheaper, easier to implement, and can be parallelized by pairs of focal points due to the integral over the acquisition surface $\partial\mathbb{D}_0$. This is very useful when dealing with large volumes of field data. In contrast, the MDD method requires inverting an integral over the redatuming level $\partial\mathbb{D}_i$, such that it does not allow for this parallelization. Also, we will now show that the double-focusing method is particularly suitable for an adaptive implementation. We can write the iterative retrieval of the wavefields $\widehat{G}^{-}$ and $\widehat{f}^{+}$ as a series:

$$\begin{aligned}\widehat{G}^{-}(\mathbf{x}_F,\mathbf{x}_S,t)&=\sum_{i=0}^{\infty}\widehat{G}^{-}_i(\mathbf{x}_F,\mathbf{x}_S,t)\\&=\Psi(\mathbf{x}_F,\mathbf{x}_S,t)\mathcal{R}\sum_{i=0}^{\infty}\Omega^i\widehat{f}^{+}_0(\mathbf{x}_S,\mathbf{x}_F,t)\end{aligned} \quad (12)$$

and

$$\begin{aligned}\widehat{f}^{+}(\mathbf{x}_S,\mathbf{x}'_F,t)&=\sum_{j=0}^{\infty}\widehat{f}^{+}_j(\mathbf{x}_S,\mathbf{x}'_F,t)\\&=\sum_{j=0}^{\infty}\Omega^j\widehat{f}^{+}_0(\mathbf{x}_S,\mathbf{x}'_F,t),\end{aligned} \quad (13)$$

where i and j denote the iteration numbers. Here, operator Ω represents the four separate operations:

$$\Omega=\theta(\mathbf{x}_F,\mathbf{x}_S,t)\mathcal{R}^{\star}\theta(\mathbf{x}_F,\mathbf{x}_S,t)\mathcal{R}. \quad (14)$$

From right to left, the reflection response R is first convolved with the wavefield that it acts upon, and then the time window $\theta(\mathbf{x}_F,\mathbf{x}_S,t)$ is applied; next this is cross correlated with the reflection response R, and then we finally apply the time window $\theta(\mathbf{x}_F,\mathbf{x}_S,t)$ again. Hence, equations 12 and 13 repeatedly convolve and correlate the reflection response with itself.

When studying the individual terms of the wavefields $\widehat{G}^{-}$ and $\widehat{f}^{+}$ that we obtain throughout the iterations, we see why the double-focusing

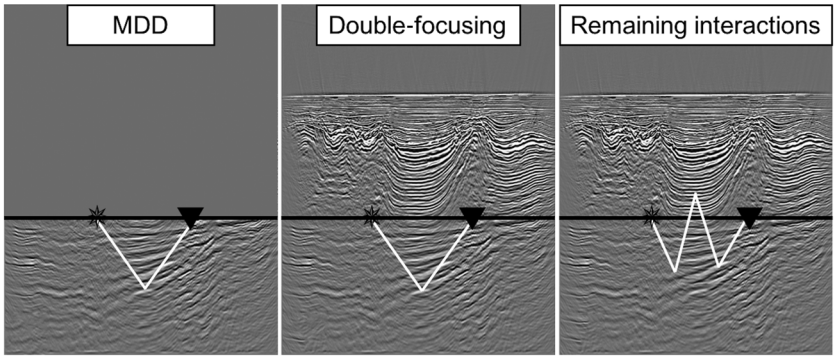

Figure 3. (a) Rays illustrating the result of source-receiver redatuming using the MDD method, in which the redatumed reflection response exists in a truncated medium, (b) rays illustrating the result of source-receiver redatuming in the physical medium using the adaptive double-focusing method, and (c) rays illustrating the remaining interactions with the overburden that result from redatuming in the physical medium instead of in the truncated medium.

method is suitable for adaptive subtraction. The upgoing Green's function $\widehat{G}^{-}$ consists of an initial wavefield $\widehat{G}_0^-$ and updates $\widehat{G}_1^-$, $\widehat{G}_2^-$, etc. The initial wavefield $\widehat{G}_0^-$ already contains all of the correct physical arrivals in combination with all the orders of internal multiples from the overburden. The first update $\widehat{G}_1^-$ contains the most important of these multiple events with opposite polarity (so-called counter events), such that addition to the initial term $\widehat{G}_0^-$ eliminates the original events. However, the amplitudes of the counter events in $\widehat{G}_1^-$ are not correct yet. The following iterations will update the amplitudes of these counter events until they completely match the amplitudes of the original events, ensuring that they completely remove the internal multiples. We observe a similar story for the individual terms of the downgoing focusing function $\widehat{f}^{+}$. The wavefield $\widehat{f}_0^+$ that is used to initiate the scheme already contains all physical information. The term $\widehat{f}_1^+$ gives the first estimate of the coda $\widehat{f}_m^+$ that is needed to complement the direct wavefield $\widehat{f}_0^+$ to account for the internal multiples generated in the overburden. It already contains the most important events, but with incorrect amplitudes. Updates of the coda, as provided by next iterations, modify these amplitudes until they are correct.

From these observations, we conclude that the two wavefields used in the double-focusing method already contain counter events to the most important internal multiples from the overburden after two iterations of solving the two coupled Marchenko equations, but with incorrect amplitudes. The amplitude updates that are normally provided by further iterations can be replaced by an adaptive filter that corrects for the amplitude mismatch between multiples and their counter events. Therefore, we can only take the first two terms of the wavefields $\widehat{G}^{-}$ and $\widehat{f}^{+}$ to write the double-focusing method as a series:

$$
\begin{aligned}
&\widehat{\widehat{G}}^{-+}(\mathbf{x}_F, \mathbf{x}'_F, t) = \\
&\sum_{i=0}^{\infty}\sum_{j=0}^{\infty}\int_{\partial\mathbb{D}_0} \widehat{G}_i^-(\mathbf{x}_F, \mathbf{x}_S, t) * \widehat{f}_j^+(\mathbf{x}_S, \mathbf{x}'_F, t) d^2\mathbf{x}_S \\
&\approx \int_{\partial\mathbb{D}_0} \widehat{G}_0^-(\mathbf{x}_F, \mathbf{x}_S, t) * \widehat{f}_0^+(\mathbf{x}_S, \mathbf{x}'_F, t) d^2\mathbf{x}_S \\
&+ \int_{\partial\mathbb{D}_0} \widehat{G}_1^-(\mathbf{x}_F, \mathbf{x}_S, t) * \widehat{f}_0^+(\mathbf{x}_S, \mathbf{x}'_F, t) d^2\mathbf{x}_S \\
&+ \int_{\partial\mathbb{D}_0} \widehat{G}_0^-(\mathbf{x}_F, \mathbf{x}_S, t) * \widehat{f}_1^+(\mathbf{x}_S, \mathbf{x}'_F, t) d^2\mathbf{x}_S. \qquad (15)
\end{aligned}
$$

Here, the first term resembles the result of conventional redatuming by using the wavefield $\widehat{f}_0^+$ for the receiver and source redatuming. This wavefield contains all primaries and all internal multiples. The second and third terms contain counter events for the first-order internal multiples on the receiver side and the source side, respectively, generated in the overburden. Note that these terms aim to remove the internal multiples that typically generate the most dominant artifacts in the image of the target area. However, some first and higher-order internal multiples remain. Analogous to the MDD method, we do not remove internal multiples generated in the target area. However, unlike the MDD method, interactions between the target and the overburden remain because the redatumed wavefield $\widehat{\widehat{G}}^{-+}(\mathbf{x}_F, \mathbf{x}'_F, t)$ exists in the physical medium instead of in the truncated medium that results from the MDD method (see Figure 3a and 3b). Double focusing creates downward-radiating sources and upward-measuring receivers at the redatuming level; hence, waves that propagate from the virtual source downward into the reservoir, reflect back up into the overburden, reflect back down into the target, and then reflect up again until sensed by the virtual receiver will remain (Figure 3c). This can be an issue depending on the geology of the area (e.g., the structure of the overburden and the depth and the thickness of the reservoir). In the Santos Basin, these remaining internal multiples arrive later than the reservoir and thus do not cause significant artifacts in its image. Note that source-receiver redatuming in the physical medium also has an advantage: The resulting redatumed reflection response can serve as input for further processing, for example, a target-oriented velocity analysis (Mildner et al., 2017) or to create target-enclosed extended images (van der Neut et al., 2017).

The success of this second focusing step (and also the MDD method, or any other method that might be used to achieve source redatuming) depends on the quality of the input wavefields that result from the first focusing step. The more iterations of the Marchenko scheme that are needed, the more the data are convolved and correlated with themselves (see equations 12 and 13), and the faster the quality will degrade when the data are imperfect, for example, in the case of a band limitation (due to the incorrect removal of an unknown source signature) or incomplete data. For this reason, the terms in equation 15 have been obtained by convolving and correlating the data with themselves no more than twice. We excluded the term $\widehat{G}_1^-(\mathbf{x}_F, \mathbf{x}_S, t) * \widehat{f}_1^+(\mathbf{x}_S, \mathbf{x}'_F, t)$ from equation 15 because it is obtained by convolving and correlating the data with itself more than twice. This higher-order term would have provided counter events for internal multiples on the source and the receiver side. Typically, these are weaker than the first-order multiples already removed by the other terms in the approximation of equation 15. Because the inclusion of this higher order term brings a risk of degrading the data quality, while typically only removing weaker internal multiples, we decided not to include this term. However, the approximation in equation 15 can in principle be extended with more terms, which can be advantageous in specific cases, depending on the geology and the data quality.

Note that we use an adaptive filter to ensure the correct and complete removal of the internal multiples by their counter events. Such a filter also adds extra robustness to the method because the adaptive subtraction might be capable of correcting for an amplitude mismatch in the updates caused by incomplete data, attenuation, or inaccurate removal of the source signature (van der Neut and Wapenaar, 2016). When the adaptive double-focusing method is correctly performed, it should essentially remove the most dominant internal multiples from the overburden that interfere with the primaries in the target area. We remark that the MDD method can be similarly written as a series to make it suitable for adaptive subtraction (van der Neut and Wapenaar, 2016). However, the computation of this series is still expensive due to the need for a densely sampled array of focal points at the redatuming level $\partial\mathbb{D}_i$, which is often unnecessary for following the processing steps (e.g., migration). In contrast, the double-focusing method requires integration over the acquisition level $\partial\mathbb{D}_0$, which gives us the freedom to select our focal points based on the requirements for further processing and the selection of the area of interest. Furthermore, double-focusing gives us the possibility to apply adaptive subtraction either in the image domain or in the redatumed data domain, such that the result can be either an image or a redatumed reflection response that can be used as input for further processing.

APPLICATION TO 2D SYNTHETIC DATA

To demonstrate the concept of the adaptive double-focusing method, tests on synthetic data and field data are performed. The synthetic data and the field data used in this paper are from the Santos Basin in Brazil. To make the synthetic tests as realistic as possible, and thus to predict the behavior of the method on field data as accurately as possible, data are generated in a model obtained from an acoustic inversion of field data. The reflection response is modeled with 601 shots, using 601 colocated sources and receivers with spacing of 25 m. An Ormsby wavelet with a central frequency of 35 Hz is convolved with the data to simulate a band limitation. Figure 1a displays an RTM image of the stratified salt and the reservoir below, created with synthetic data. The target area, which is below the base of salt, contains artifacts due to internal multiples generated in the complex overburden that overlie the primary reflectors that we wish to see. To see what these artifacts look like, Figure 1b displays the same area in the Santos Basin, but now the model is homogeneous below the base of salt. As a result, reflections from the reservoir do not exist and only the artifacts due to scattering in the overburden are visible in the region below the base of the salt. Note that most multiples have a half-circle appearance, showing an imprint of the salt above. Based on these images, it is clear that the removal of internal multiples is necessary to get a clear image of the target, which can possibly aid the geologic interpretation in the area.

We start by applying the Marchenko method on 2D synthetic data of the Santos Basin. It is important to correctly design the time window $\theta(\mathbf{x}_F, \mathbf{x}_S, t)$ that is used to retrieve the receiver-redatumed wavefields with the Marchenko method. In particular, a choice of parameters t_d and t_e has to be made (see equation 5). The choice of t_d is based on the smooth velocity model, but the choice of t_e is not that straightforward, yet it is crucial for the successful adaptive source redatuming that follows the single-focusing Marchenko method. We refer the reader to Appendix A for an explanation on how to correctly do this.

After performing two iterations of the Marchenko scheme with a correct time window, we convolve the individual terms of $\widehat{G}^{-}$ and $\widehat{f}^{+}$ with each other according to equation 15. The result can be seen in Figure 4. Remember that the first term contains primaries and all orders of internal multiples, whereas the second and third terms contain counter events for the most dominant internal multiples that were generated in the overburden.

We continue by applying adaptive subtraction to retrieve the redatumed wavefield $\widehat{G}^{-+}(\mathbf{x}_F, \mathbf{x}'_F, t)$. This can be done in multiple ways and in multiple domains. We apply adaptive subtraction in the curvelet domain (e.g., Wu and Hung, 2015) because it provides an extra degree of freedom compared with the space-time domain. Curvelets have a location, a scale, and a dip separation. The dip separation is the extra degree of freedom that can make a difference in distinguishing between primaries and multiples. The curvelet domain handles the curved and linear events better, particularly when a primary and a multiple overlap in time and space, but not in dip. The used filter is a least-squares matching filter that minimizes the mismatch between the terms in a least-squares sense. This can be a single scalar for all events, or more likely, a different scalar for each event when a nonstationary mismatch is present. A note of caution is relevant here: Even though we are using an adaptive filter in the curvelet domain, care has to be taken not to remove the primaries together with the multiples.

Figure 5 shows the source-receiver-redatumed reflection responses that result from applying the MDD method and the adaptive double-focusing method to 2D synthetic data of the Santos Basin. The MDD method and the adaptive double-focusing method use wavefields that result from two iterations of the Marchenko method. Figure 5a shows the modeled redatumed reflection response for comparison. It has been obtained in a medium that is homogeneous above the redatuming level such that the overburden does not exist. The white lines indicate the mute that is applied to remove the acausal wavefields. When comparing the results of the MDD method and the adaptive double-focusing method with the modeled reflection response, it is clear that the adaptive double-focusing method delivers a reflection response that resembles the modeled response more closely. The MDD method seems to suffer from high-frequency remnants of multiples or high-frequency noise due to the required inversion. We remark that the result of the MDD method can be improved by using more iterations of the Marchenko scheme. However, this comes at a cost and might result in a quality degradation of the data.

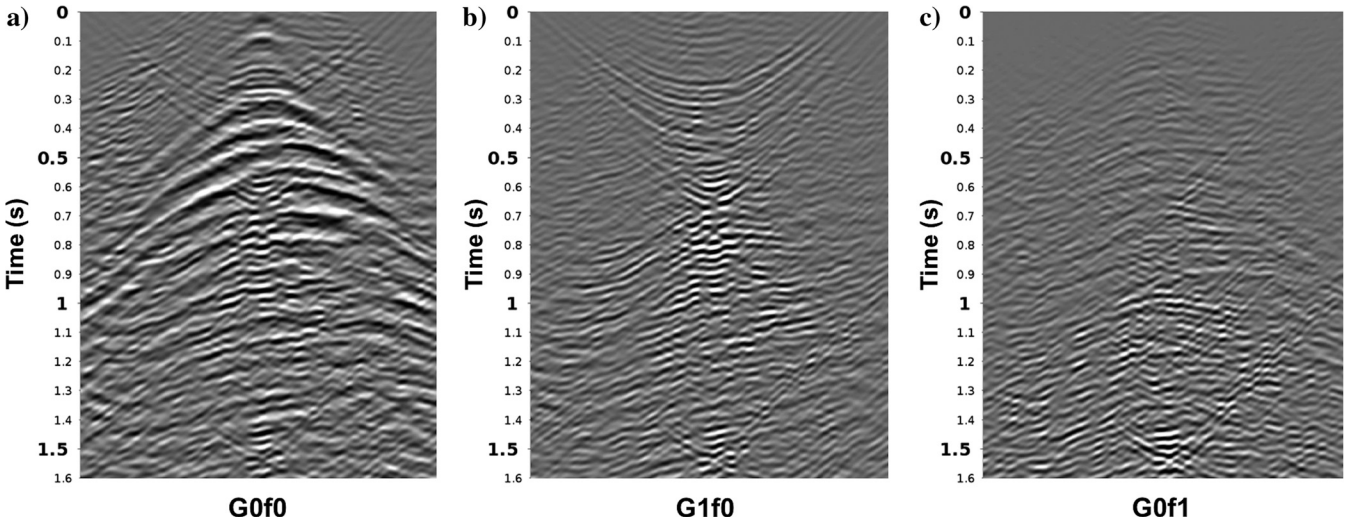

Figure 4. Individual terms from equation 15 in the synthetic example of the Santos Basin. (a) The primaries and internal multiples and (b and c) counter events for the most dominant internal multiples that were generated in the overburden.

Using the same amount of iterations, the adaptive double-focusing method provides a cleaner redatumed reflection response. Despite the fact that a full medium truncation has not been achieved, multiples originating from the remaining interactions between the target and the overburden (as depicted in Figure 3c) seem to be negligible.

Figure 6 shows the images obtained after applying an RTM to the redatumed reflection responses in Figure 5. It also contains an image of directly applying an RTM to the reflection response at the acquisition surface $\partial\mathbb{D}_0$. The artifacts in the image due to internal multiples can be seen in the shape of half-circles as spotted earlier in Figure 1. These artifacts are no longer present in the RTM images after applying the MDD method and the adaptive double-focusing method. Both methods remove the artifacts well, but the adaptive double-focusing method produces a slightly cleaner image that resembles the image of the modeled reflection response more closely (as indicated by the arrows).

Sensitivity to an unknown scaling factor

Next, we continue by verifying whether the proposed method is less sensitive to imperfections in the (preprocessed) data than the MDD method. A typical shortcoming of field data is an unknown scaling of the source strength (Ravasi et al., 2016). So far, we have assumed that $R(\mathbf{x}_R, \mathbf{x}_S, t)$ is the real reflection response of the subsurface, but this is not the case in reality. We only have access to a reflection response that is scaled by an unknown factor that depends on the acquisition and the preprocessing (e.g., the deconvolution of the (unknown) source signature). We compare the performance of the MDD method and the adaptive double-focusing method for the most simple error in scaling: a reflection response multiplied by a single scalar. We test values of 0.5 and 2.0. The resulting redatumed responses can be found in Figure 7.

When scaling the reflection response by a factor of 0.5, the MDD method has problems removing internal multiples. In contrast, the adaptive filter applied to the double-focusing method corrects for

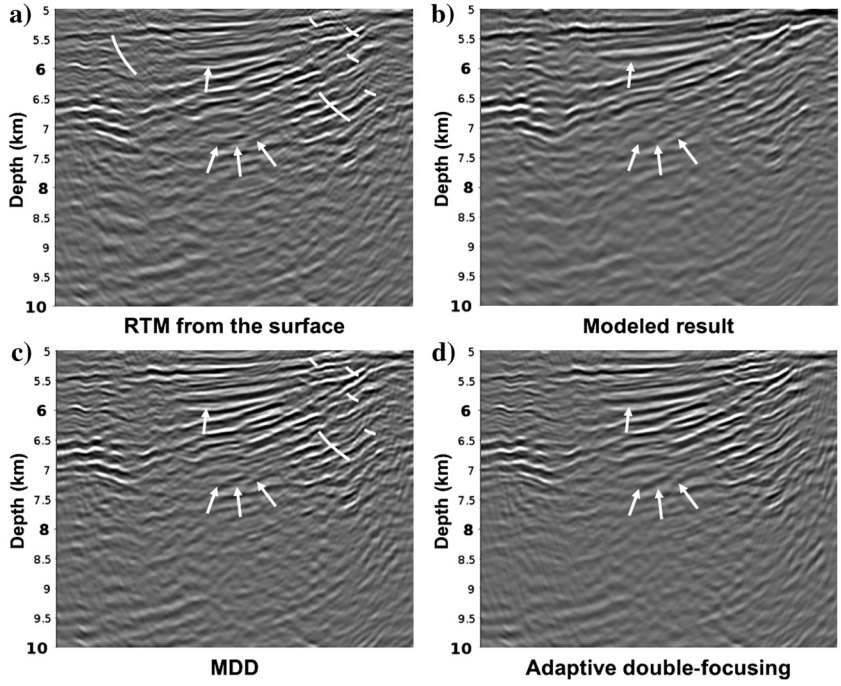

Figure 6. Images resulting from the application of the MDD method and the adaptive double-focusing method to 2D synthetic data of the Santos Basin. (a) RTM image obtained from data at the acquisition surface, magnified at the target. All primaries and artifacts due to internal multiples are present. (b) RTM image of a modeled redatumed reflection response, obtained in a medium that is homogeneous above the redatuming level. (c) RTM image resulting from the MDD method. (d) RTM image resulting from the adaptive double-focusing method.

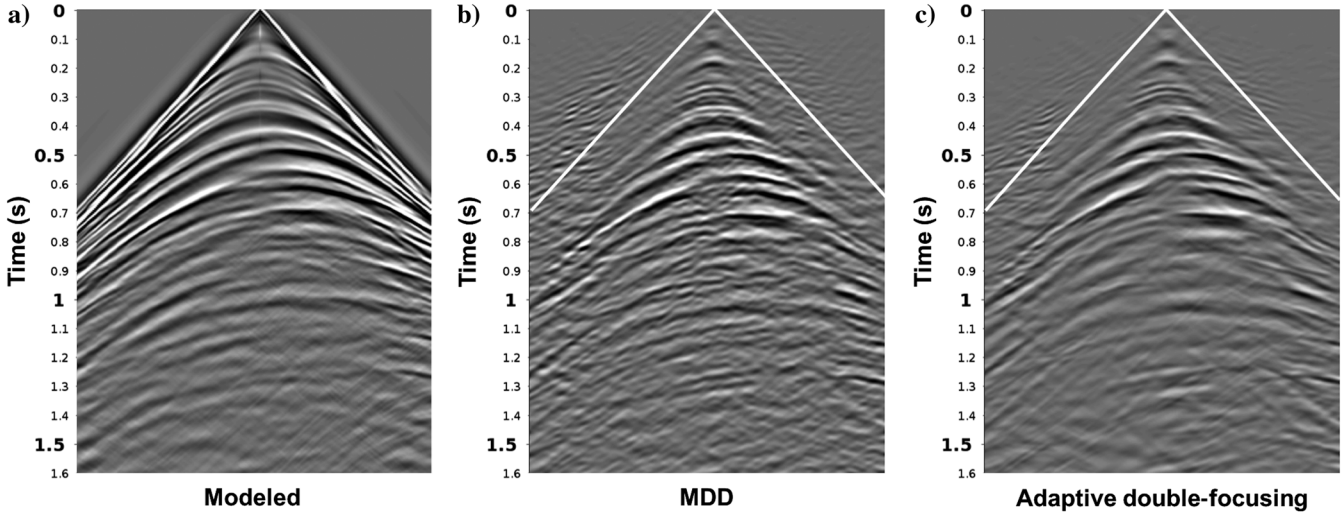

Figure 5. (a) Redatumed reflection response obtained by modeling in a medium that is homogeneous above the redatuming level, (b) the MDD result, and (c) the result of the adaptive double-focusing method. The MDD method and the adaptive double-focusing method use two iterations of the Marchenko scheme.

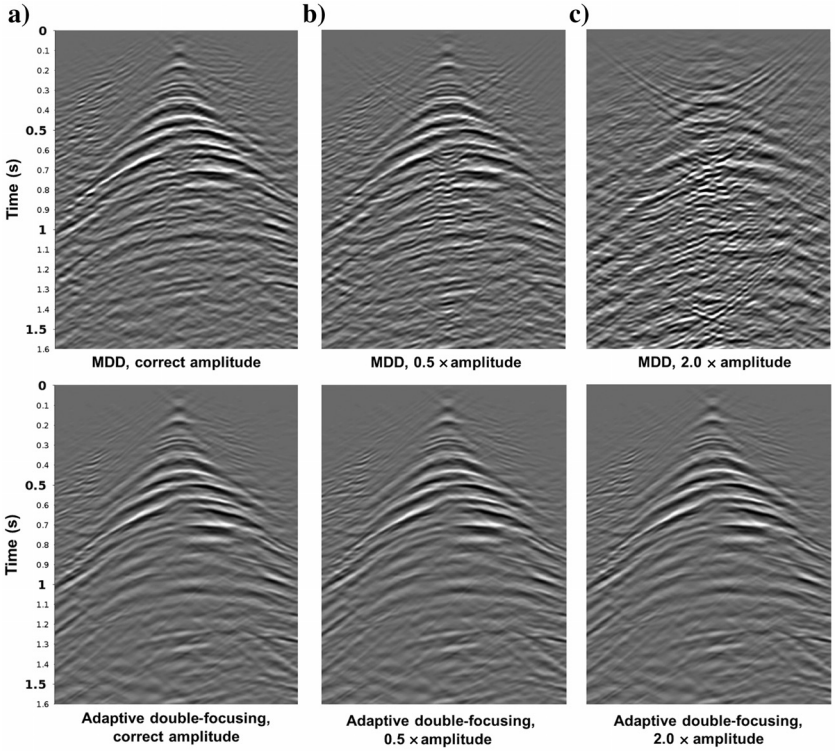

Figure 7. Comparison of the MDD method and the adaptive double-focusing method for an unknown scaling of source strength. (a) The results with a known scaling factor, (b) the results when the reflection response is multiplied by 0.5, and (c) the results when the reflection response is multiplied by 2.0. The adaptive double-focusing method is not affected by the presence of such a scalar, whereas the MDD method is.

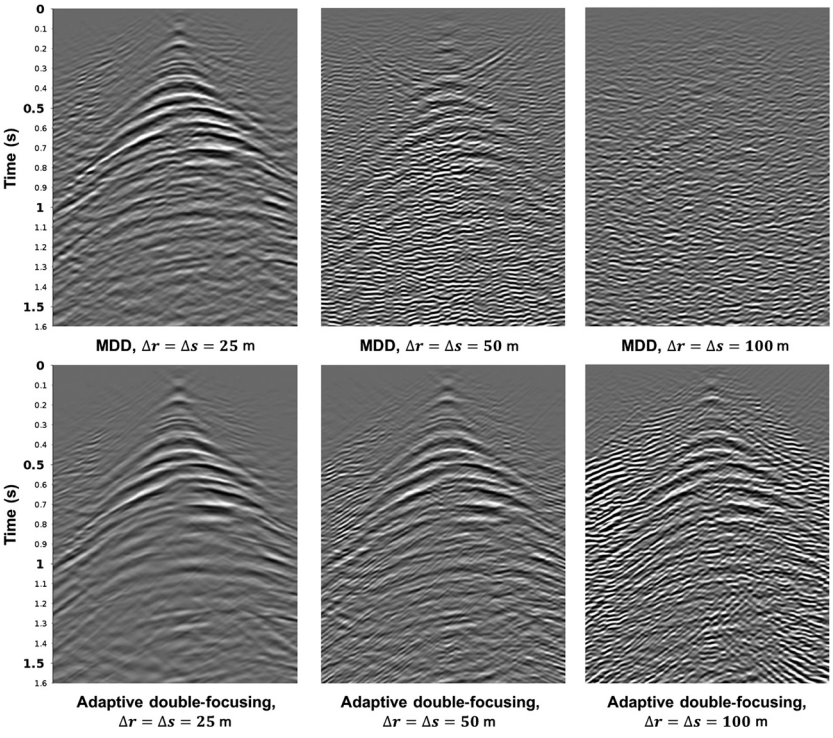

Figure 8. Comparison of the MDD method and the adaptive double-focusing method for a coarser acquisition geometry, using two iterations of the Marchenko scheme. Both methods suffer, but adaptive double-focusing is less sensitive.

this error in scaling. When multiplying the amplitudes of the reflection response by a factor 2.0, the MDD method starts adding multiples instead of removing them. Again, the adaptive filter corrects for the erroneous scaling factor. This shows that the adaptive double-focusing method is more robust and less sensitive to imperfections in the preprocessed data. In theory, the result of the MDD method can be improved by using other methods that estimate the unknown scaling factor (Brackenhoff, 2016). However, these methods do not always result in the correct answer and only provide an estimate at an additional computational cost. In contrast, the adaptive double-focusing method implicitly takes care of issues related to an unknown scaling factor.

Sensitivity to a less dense source and receiver spacing

In reality, a perfect acquisition geometry does not exist. Therefore, it is important that the adaptive double-focusing method is capable of obtaining an acceptable result when the source and receiver spacing is coarser than the 25 m used to generate the synthetic data. Figure 8 shows the redatumed reflection responses obtained by applying the MDD method and the adaptive double-focusing method when increasing the source and receiver spacing from 25 to 50 m and to 100 m. The MDD method greatly suffers and has problems recovering the primary signal with a coarser acquisition geometry. The adaptive double-focusing method also suffers, but it still manages to obtain a reasonable amount of primary energy.

Figure 9 shows a comparison of the RTM images of the MDD method and the adaptive double-focusing method with source and receiver spacing of 50 m. The adaptive double-focusing method has removed significantly more artifacts due to internal multiples than the MDD method. By replacing the inversion of the MDD method by a second focusing step, we have created a source-redatuming method that is more capable of handling a sparse acquisition geometry.

APPLICATION TO 2D FIELD DATA

We continue by applying the adaptive double-focusing method to 2D field data. The data were acquired in the same region as covered by the synthetic data. The acquisition was performed with six streamers, having a cable spacing of 150 m and a cable length of 6000 m. We regularize the shot and receiver positions on the same line with spacing of 25 m. To satisfy the assumptions underlying the Marchenko scheme, the data are preprocessed using denoise, designature, deghosting, and surface-related multiple attenuation. Figure 10a shows the RTM image obtained

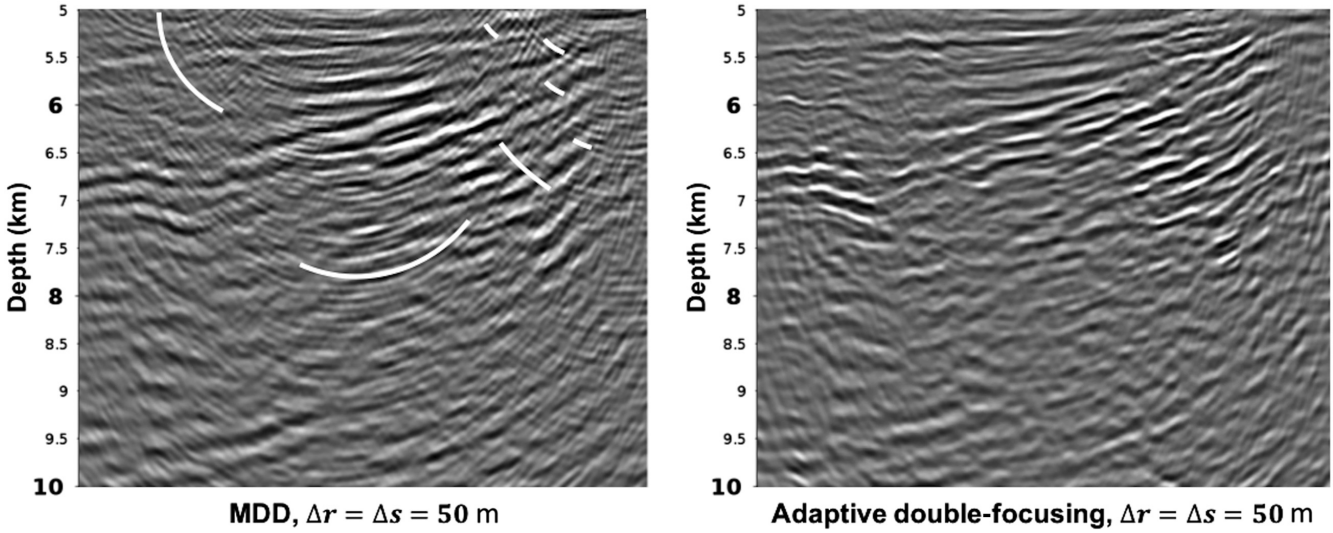

Figure 9. The RTM images of the MDD method and the adaptive double-focusing method for a source and receiver spacing of 50 m. The image of the result of the MDD method shows many artifacts, whereas the adaptive double-focusing method has still managed to remove a significant amount of these artifacts despite the coarse acquisition geometry.

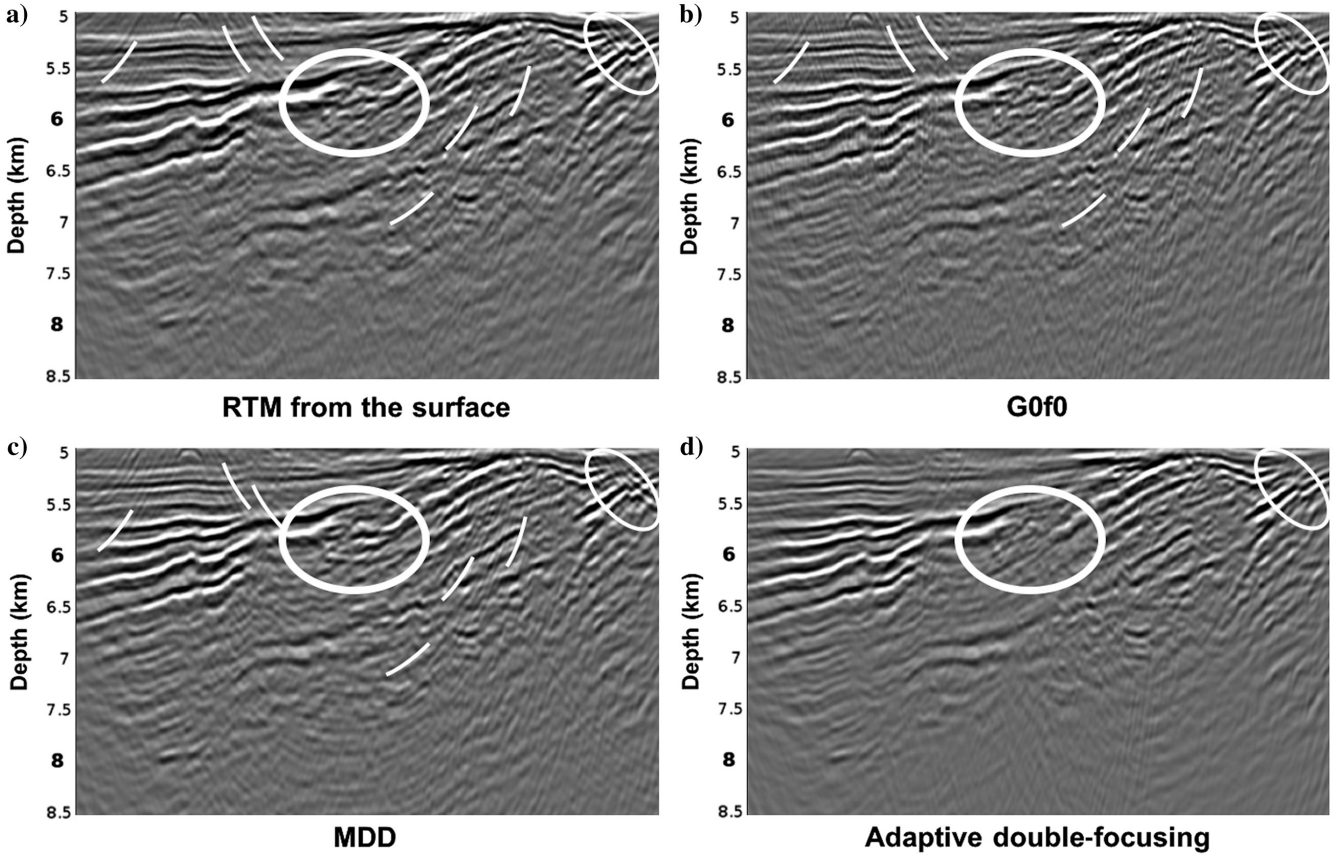

Figure 10. Images resulting from the application of the MDD method and the adaptive double-focusing method to 2D field data of the Santos Basin. (a) RTM image obtained from data at the acquisition surface, magnified at the target. All primaries and artifacts due to internal multiples are present. (b) RTM image of the first term of the adaptive double-focusing method. (c) RTM image resulting from the MDD method. (d) RTM image resulting from the adaptive double-focusing method.

from the reflection response acquired at the acquisition surface $\partial\mathbb{D}_0$. We call this the result of conventional imaging, in which internal multiples from the overburden create artifacts in the target zone. Figure 10b shows the RTM image of the first term of the adaptive double-focusing method. This term includes primaries and artifacts due to internal multiples from the overburden, and it is comparable to the result of the RTM from the acquisition surface. Figure 10c shows the result of applying the MDD method. It did not succeed in removing the multiples, but it seems to have boosted their amplitudes instead. This is comparable to what we observed in Figure 7. Figure 10d shows the result of applying the adaptive double-focusing method to this data set. The white circles and lines indicate areas that clearly show the effect of multiple removal. The thick white circle highlights the most significant improvement in the image: The application of our method has improved the geologic interpretability in the area. The half-circles due to multiples that we first encountered in the synthetic data (Figure 1) have given the thick encircled section in the other images of Figure 10a a different appearance, masking the real structure below. This masked structure becomes visible after application of the adaptive double-focusing method.

CONCLUSION

We presented the adaptive double-focusing method as an alternative for the MDD method to apply source-receiver Marchenko redatuming to field data. Double focusing is created by introducing a second focusing step that naturally complements the first focusing step of the single-focusing Marchenko method. The used wavefields and the integral over the acquisition surface make it particularly suitable for adaptive subtraction, resulting in the adaptive double-focusing method. This method predicts and removes the most dominant internal multiples generated in the overburden. Not only is this method less sensitive to imperfections in the data and the acquisition geometry than the MDD method, it is also computationally much cheaper and allows for parallelization over pairs of focal points, making it suitable for application to large data volumes. Furthermore, it produces improved results over the MDD method when using wavefields resulting from the same amount of Marchenko iterations. Using the adaptive double-focusing method, we have been able to successfully apply source-receiver Marchenko redatuming to field data of the Santos Basin. The resulting RTM image shows that we have correctly predicted and subtracted the dominant internal multiples originating from the overburden. We have thereby improved the geologic interpretability in the target area, despite using imperfect data and a sparse acquisition geometry. Based on this result, we conclude that the proposed method is an effective tool for applying source-receiver Marchenko redatuming to field data.

ACKNOWLEDGMENTS

This research was performed in the framework of the project "Marchenko imaging and monitoring of geophysical reflection data," which is part of the Dutch Open Technology Programme with project number 13939 and is financially supported by NWO Domain Applied and Engineering Sciences. The research of K. Wapenaar has received funding from the European Research Council (ERC) under the European Union's Horizon 2020 research and innovation programme (grant agreement no. 742703). We thank CGG Rio de Janeiro for a fruitful collaboration and M. Peiro for preparing the model used to create the synthetic 2D data for the tests. We also thank M. Ravasi, A. Jia, and two anonymous reviewers for their help in improving this manuscript. Also, we are grateful for discussions with J. Brackenhoff, L. Zhang, M. Dukalski and I. Vasconcelos.

DATA AND MATERIALS AVAILABILITY

Data associated with this research are confidential and cannot be released.

APPENDIX A

DESIGN OF THE TIME WINDOW θ FOR THE ADAPTIVE DOUBLE-FOCUSING METHOD

The first step of the adaptive double-focusing method, single focusing by iteratively solving the coupled Marchenko equations,

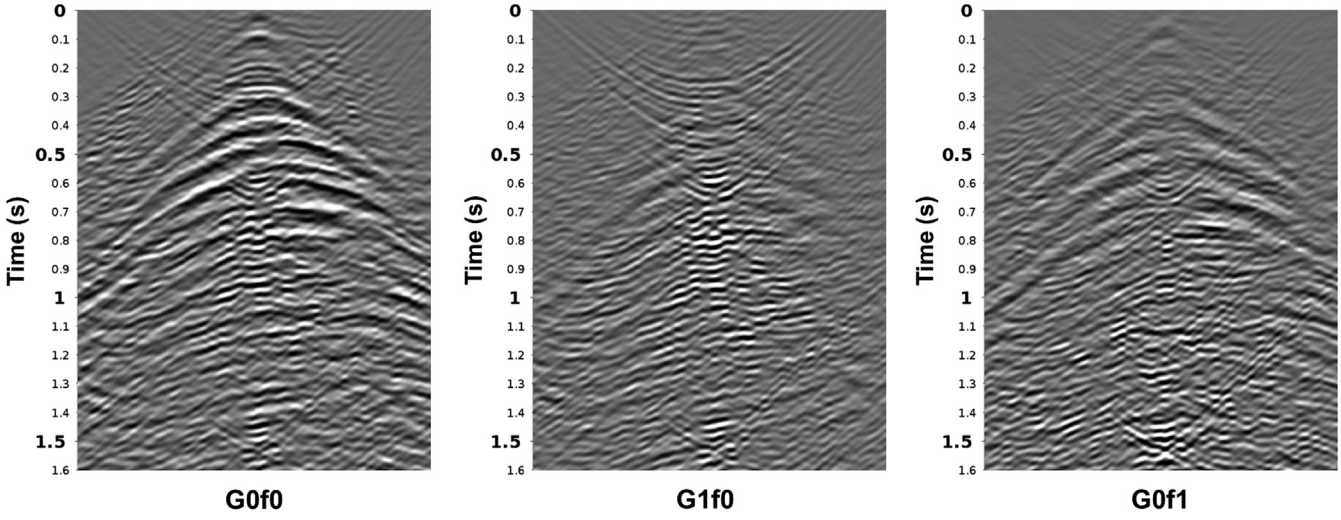

Figure A-1. Common-shot gathers of the individual terms in equation 15 for an erroneously small t_e in the Marchenko method. The source is located in the middle of the array of focal points at the redatuming level.

requires designing a time window $\theta(\mathbf{x}_F, \mathbf{x}_S, t)$ to correctly retrieve the wavefields needed for source redatuming. This window is designed by choosing parameters t_d and t_ϵ (see equation 5). The choice of t_d is based on the smooth velocity model, but the choice of t_ϵ is not that straightforward. We will explain how the choice of t_ϵ affects the adaptive double-focusing method and how we can make a correct choice.

A rule of thumb is to set t_ϵ equal to half the duration of the zero-phase wavelet convolved with the direct wave $\widehat{f}_0^+$. This holds for synthetic data in 1D, but it does not always hold for 2D and 3D data with a finite aperture. If using the rule of thumb, we estimate a t_ϵ of 14.3 ms for the 2D synthetic data of the Santos Basin. When taking a t_ϵ that is smaller than this estimation, we retrieve the wavefields in Figure A-1. Note that the first term should contain primaries and all orders of internal multiples, whereas the second and third terms should only contain counter events for the most dominant internal multiples generated in the overburden. However, when looking closely at the events in all three terms, the second and third terms have events that appear to be the result of "primary leakage." They seem to contain a copy of the correct events in the first term that should remain intact. If we use these incorrectly retrieved wavefields for adaptive subtraction, the damage of the primary will be severe: The second and third terms will remove the primaries together with the multiples.

We will now show that the apparent primary leakage in the data of the Santos Basin is actually the result of an incorrect choice of t_ϵ, and it can thus be avoided. Figure A-2 shows the truncations in the time domain during the two steps that comprise a single iteration of the Marchenko scheme (equations 3 and 4). When looking at the wavefields that result from evaluating equation 3, the upgoing focusing function $\widehat{f}^-$ can be found before t_d (the traveltime of the direct wavefield from the focal point to the acquisition surface) and the upgoing Green's function $\widehat{G}^-$ can be found after t_d. The actual truncation applied by time window $\theta(\mathbf{x}_F, \mathbf{x}_S, t)$ is made at $t_d - t_\epsilon$, so it is slightly before t_d.

The evaluation of equation 4 results in the coda of the polarity- and time-reversed downgoing Green's function $\widehat{G}_m^+$ before $-t_d$ and the coda of the downgoing focusing function $\widehat{f}_m^+$ after $-t_d$. However, the updates of the direct wave of the downgoing Green's function $\widehat{G}_d^+(-t)$ arrive exactly at $-t_d$ (see the gray-colored arrival in Figure A-2). In this situation, the time window $\theta(\mathbf{x}_F, \mathbf{x}_S, t)$ applies the truncation slightly after $-t_d$, at $-t_d + t_\epsilon$.

When now studying the retrieval of the individual terms $\widehat{G}_0^-$, $\widehat{G}_1^-$, and $\widehat{f}_1^+$ from equation 15 in detail, while keeping Figure A-2 in mind, the issue becomes clear. Note that $\widehat{f}_0^+$ is a known that is unaffected by the truncations. The wavefield $\widehat{G}_0^-$ is retrieved during the first iteration by computing $\widehat{G}_0^- = \Psi\mathcal{R}\widehat{f}_0^+$. No matter how small t_ϵ is chosen, the truncation will never be placed later than t_d, and it will thus never incorrectly place parts of the upgoing focusing function $\widehat{f}^-$ into this Green's function. Therefore, our first term, containing $\widehat{G}_0^-$ and $\widehat{f}_0^+$, should not suffer from a t_ϵ that was chosen too small.

The story is different for the second and third terms in equation 15. The third term contains the wavefield $\widehat{f}_1^+$ that is retrieved by $\widehat{f}_1^+ = \theta\mathcal{R}^\star\widehat{f}_0^-$. Now the truncation does matter because a t_ϵ that is chosen too small will result in an $\widehat{f}_1^+$ that also contains part of the update of the direct downgoing Green's function $\widehat{G}_d^+(-t)$ (see Figure A-2). This update arrives at the exact same time as wavefield $\widehat{f}_0^+$ and it will therefore act as a scaled version of this wavefield. As a result, we do not retrieve $\widehat{f}_1^+$, but we obtain $\widehat{f}_1^+ + \alpha\widehat{f}_0^+$ for a t_ϵ that is too small. When then performing the convolution of $\widehat{G}_0^-$ and $\widehat{f}_1^+$ to compute the third term, we obtain $\widehat{G}_0^- * (\widehat{f}_1^+ + \alpha\widehat{f}_0^+)$ instead, which is equal to adding a scaled version of the first term to the third term. As a result, we see the same primaries as found in the first term also in the third term for an erroneously small t_ϵ.

When now continuing with our incorrectly retrieved $\widehat{f}_1^+$, such that it is actually $\widehat{f}_1^+ + \alpha\widehat{f}_0^+$, the next step is the retrieval of the wavefield $\widehat{G}_1^-$. This is the first update of the wavefield $\widehat{G}_0^-$, which can be written as $\widehat{G}_1^- = \Psi\mathcal{R}\widehat{f}_1^+$ (see equation 8). Using our incorrect $\widehat{f}_1^+ = \widehat{f}_1^+ + \alpha\widehat{f}_0^+$, we now obtain $\widehat{G}_1^- = \Psi R * (\widehat{f}_1^+ + \alpha\widehat{f}_0^+) = \widehat{G}_1^- + \alpha\widehat{G}_0^-$. Therefore, the retrieved $\widehat{G}_1^-$ has an imprint of $\widehat{G}_0^-$, which explains the primary leakage that is also observed in the second term.

Thus, finding a correct t_ϵ is essential for the successful application of adaptive subtraction in the double-focusing method. It would seem straightforward to just choose a very large value for t_ϵ, but this can result in an incomplete solution. The choice of t_ϵ defines the smallest period of internal multiple that can be resolved. The shorter the period of the internal multiples, the closer the coda $\widehat{f}_m^+$ will follow the direct wave $\widehat{f}_0$. Thus, the larger the choice of t_ϵ, the higher the risk of incorrectly muting part of the focusing functions. When incorrectly muted, not all internal multiples will be constructed, and they cannot be subtracted. This is something that should not be taken lightly because this is the purpose of applying source-receiver redatuming to the reflection response. Instead of using trial and error to find a suitable value for t_ϵ, the autocorrelation of the reflection response R can serve as an indication. Figure A-3 shows the autocorrelation of the synthetic reflection response. The autocorrelation of the individual events can be found on the zero lag. Correlations of different events with each other can be found elsewhere in time. The correlation of a short period internal multiple with a primary generated by the same reflector will appear close to the zero lag because there is only a small difference in traveltime. Therefore, the time in between the arrival at the zero lag and the next arrival is an indication of the shortest period internal multiples that are present in the data. This can be used as a guide to define an upper bound for t_ϵ, whereas visual inspection for primary leakage can be used to set a lower bound. When the upper bound is below the lower bound, short period internal multiples may have to be sacrificed to ensure a correct adaptive subtraction. Note that reflection response R should not have a source signature when autocorrelating it; otherwise, this method is not reliable. We also remark that this explanation holds for the first-order internal multiples as observed in the data of the Santos Basin, where we have strong reflectors from the salt with weaker reflectors below. The explanation might not hold when more (strong) reflectors are involved.

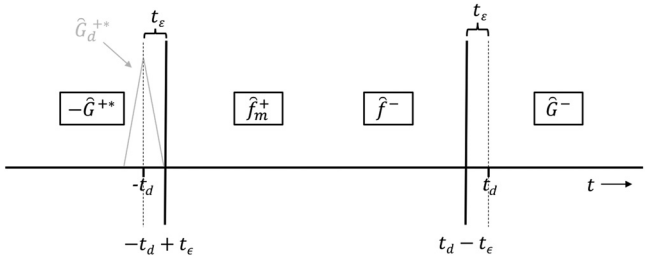

Figure A-2. Illustration of the truncations imposed by the filter θ in the Marchenko method, for a focusing depth that is sufficiently far away from a reflector.

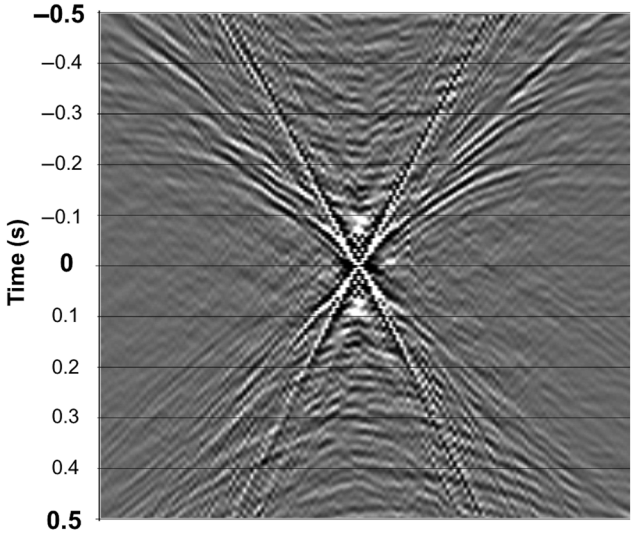

Figure A-3. Auto-correlation of the synthetic reflection response of the Santos Basin.

In this paper, we have applied adaptive subtraction to the individual terms of the double-focusing method in Figure 4. They were retrieved by chosing a t_ϵ of 100 ms.

REFERENCES

Amundsen, L., L. T. Ikelle, and L. E. Berg, 2001, Multidimensional signature deconvolution and free-surface multiple elimination of marine multicomponent ocean-bottom seismic data: Geophysics, **66**, 1594–1604, doi: 10.1190/1.1486770.

Brackenhoff, J., 2016, Rescaling of incorrect source strength using Marchenko redatuming: M.Sc. thesis, Delft University of Technology.

Broggini, F., and R. Snieder, 2012, Connection of scattering principles: A visual and mathematical tour: European Journal of Physics, **33**, 593–613, doi: 10.1088/0143-0807/33/3/593.

Broggini, F., R. Snieder, and K. Wapenaar, 2014, Data-driven wavefield focusing and imaging with multidimensional deconvolution: Numerical examples for reflection data with internal multiples: Geophysics, **79**, no. 3, WA107–WA115, doi: 10.1190/geo2013-0307.1.

Cypriano, L., F. Marpeau, R. Brasil, G. Welter, H. Prigent, H. Douma, M. Velasques, J. Boechat, P. de Carvalho, C. Guerra, C. Theodoro, A. Martini, and J. Nunes Cruz, 2015, The impact of inter-bed multiple attenuation on the imaging of pre-salt targets in the Santos basin off-shore Brazil: 77th Annual International Conference and Exhibition, EAGE, Extended Abstracts, doi: 10.3997/2214-4609.201412691.

Davydenko, M., and D. Verschuur, 2017, Full-wavefield migration: Using surface and internal multiples in imaging: Geophysical Prospecting, **65**, 7–21, doi: 10.1111/1365-2478.12360.

Hartstra, I., C. Almagro Vidal, and K. Wapenaar, 2017, Full-field multidimensional deconvolution to retrieve body-wave reflections from sparse passive sources: Geophysical Journal International, **210**, 609–620.

Hung, B., and M. Wang, 2012, Internal demultiple methodology without identifying the multiple generators: 82nd Annual International Meeting, SEG, Expanded Abstracts, 1–5, doi: 10.1190/segam2012-0549.1.

Jakubowicz, H., 1998, Wave equation prediction and removal of interbed multiples: 60th Annual International Conference and Exhibition, EAGE, Extended Abstracts, doi: 10.1190/1.1820204.

Mildner, C., F. Broggini, J. O. Robertsson, D.-J. van Manen, and S. Greenhalgh, 2017, Target-oriented velocity analysis using Marchenko-redatumed data: Geophysics, **82**, no. 2, R75–R86, doi: 10.1190/geo2016-0280.1.

Minato, S., T. Matsuoka, and T. Tsuji, 2013, Singular-value decomposition analysis of source illumination in seismic interferometry by multidimensional deconvolution: Geophysics, **78**, no. 3, Q25–Q34, doi: 10.1190/geo2012-0245.1.

Nakata, N., R. Snieder, and M. Behm, 2014, Body-wave interferometry using regional earthquakes with multidimensional deconvolution after wavefield decomposition at free surface: Geophysical Journal International, **199**, 1125–1137, doi: 10.1093/gji/ggu316.

Ravasi, M., 2017, Rayleigh-Marchenko redatuming for target-oriented, true-amplitude imaging: Geophysics, **82**, no. 6, S439–S452, doi: 10.1190/geo2017-0262.1.

Ravasi, M., I. Vasconcelos, A. Kritski, A. Curtis, C. A. da Costa Filho, and G. A. Meles, 2016, Target-oriented Marchenko imaging of a North Sea field: Geophysical Journal International, **205**, 99–104, doi: 10.1093/gji/ggv528.

Rose, J. H., 2001, "Single-sided" focusing of the time-dependent Schrödinger equation: Physical Review A, **65**, 012707, doi: 10.1103/PhysRevA.65.012707.

Rose, J. H., 2002, "Single-sided" autofocusing of sound in layered materials: Inverse Problems, **18**, 1923–1934, doi: 10.1088/0266-5611/18/6/329.

Singh, S., and R. Snieder, 2017, Source-receiver Marchenko redatuming: Obtaining virtual receivers and virtual sources in the subsurface: Geophysics, **82**, no. 2, Q13–Q21, doi: 10.1190/geo2016-0074.1.

Slob, E., and K. Wapenaar, 2017, Theory for Marchenko imaging of marine seismic data with free-surface multiple elimination: 79th Annual International Conference and Exhibition, EAGE, Extended Abstracts, doi: 10.3997/2214-4609.201700800.

Slob, E., K. Wapenaar, F. Broggini, and R. Snieder, 2014, Seismic reflector imaging using internal multiples with Marchenko-type equations: Geophysics, **79**, no. 2, S63–S76, doi: 10.1190/geo2013-0095.1.

van der Neut, J., J. Brackenhoff, M. Staring, L. Zhang, S. de Ridder, E. Slob, and K. Wapenaar, 2018, Single-and double-sided Marchenko imaging conditions in acoustic media: IEEE Transactions on Computational Imaging, **4**, 160–171, doi: 10.1109/TCI.2017.2772440.

van der Neut, J., M. Ravasi, Y. Liu, and I. Vasconcelos, 2017, Target-enclosed seismic imaging: Geophysics, **82**, no. 6, Q53–Q66, doi: 10.1190/geo2017-0166.1.

van der Neut, J., M. Tatanova, J. Thorbecke, E. Slob, and K. Wapenaar, 2011, Deghosting, demultiple, and deblurring in controlled-source seismic interferometry: International Journal of Geophysics, **2011**, 1–28.

van der Neut, J., I. Vasconcelos, and K. Wapenaar, 2015, On Green's function retrieval by iterative substitution of the coupled Marchenko equations: Geophysical Journal International, **203**, 792–813, doi: 10.1093/gji/ggv330.

van der Neut, J., and K. Wapenaar, 2016, Adaptive overburden elimination with the multidimensional Marchenko equation: Geophysics, **81**, no. 5, T265–T284, doi: 10.1190/geo2016-0024.1.

Wapenaar, K., F. Broggini, E. Slob, and R. Snieder, 2013, Three-dimensional single-sided Marchenko inverse scattering, data-driven focusing, Green's function retrieval, and their mutual relations: Physical Review Letters, **110**, 084301, doi: 10.1103/PhysRevLett.110.084301.

Wapenaar, K., J. Thorbecke, J. van der Neut, F. Broggini, E. Slob, and R. Snieder, 2014a, Green's function retrieval from reflection data, in absence of a receiver at the virtual source position: The Journal of the Acoustical Society of America, **135**, 2847–2861, doi: 10.1121/1.4869083.

Wapenaar, K., J. Thorbecke, J. van der Neut, F. Broggini, E. Slob, and R. Snieder, 2014b, Marchenko imaging: Geophysics, **79**, no. 3, WA39–WA57, doi: 10.1190/geo2013-0302.1.

Wapenaar, K., J. van der Neut, and E. Slob, 2016, Unified double- and single-sided homogeneous Green's function representations: The Royal Society Publishing, Proceedings A, **472**, 20160162, doi: 10.1098/rspa.2016.0162.

Weglein, A. B., F. A. Gasparotto, P. M. Carvalho, and R. H. Stolt, 1997, An inverse scattering series method for attenuating multiples in seismic reflection data: Geophysics, **62**, 1975–1989, doi: 10.1190/1.1444298.

Wu, X., and B. Hung, 2015, High-fidelity adaptive curvelet domain primary-multiple separation: First Break, **33**, 53–59.